Photocatalytic activity of titanium dioxide produced by high-energy milling

Ekaterina A. Kozlova[1,2,a], Albina A. Valeeva[3,b], Anna A. Sushnikova[1,c], Angelina V. Zhurenok[2,d],
Andrey A. Rempel[1,e]

[1]Institute of Metallurgy, UB RAS, Yekaterinburg, 620016, Russia
[2]Boreskov Institute of Catalysis, SB RAS, Novosibirsk, 630090, Russia
[3]Institute of Solid State Chemistry, UB RAS, Yekaterinburg, 620108, Russia

[a]kozlova@catalysis.ru, [b]anibla_v@mail.ru, [c]sushnikova.ann@gmail.com, [d]angelinazhurenok@gmail.com,
[e]rempel.imet@mail.ru

Corresponding author: Ekaterina A. Kozlova, kozlova@catalysis.ru

ABSTRACT In this work, photocatalysts based on titanium dioxide were synthesized by high-energy ball milling of commercial titanium dioxide in the anatase modification. Using a complex of physicochemical methods, including XRD, low-temperature nitrogen adsorption, XPS and TEM, it was shown that the milling of commercial anatase leads to phase transformations and the formation of several phases of titanium dioxide, namely the high-pressure phase, the monoclinic phase of anatase and rutile, except for in addition, there is a change in the crystalline size and the value of the specific surface area grows from 8 to 31 m^2/g. It was found that defects are introduced into the system during ball milling. The photocatalysts obtained by milling showed an activity comparable to the commercial standard TiO$_2$ Degussa P25 in the destruction of the methylene blue dye under the action of UV light, while the adsorption properties of the synthesized samples exceeded those of commercial P25.

KEYWORDS Titanium dioxide, high-energy ball milling, photocatalytic oxidation

1. Introduction

Currently, the problem of water and air purification from various contaminants is very urgent [1]. The recent rapid growth of the industry led to worldwide environmental problems [2]. It is well known that dyes play an important role in various branches of textile industry. Nowdays over 100 000 commercially available synthetic dyes are usually used in industries. These dyes are mainly derived from coal tar and petroleum intermediates, with a total annual production of more than $7 \cdot 10^5$ tons [3–6].

Advanced oxidation processes (AOPs) are the most widely used technology for dye degradation. Recently, there has been a great amount of works that has been done and various kinds of AOPs have been developed [7]. At present, for the oxidation of various pollutants, including dyes, photocatalysis on semiconductors is widely used [8]. Of great interest is the photocatalytic oxidation of pesticides and detergents [9]. Photocatalytic reactions for the oxidation of pesticides such as acrinathrine, methamidophos, malathion, diazion, carbetamide, and the insecticide fenitration have already been described [9–13]. A large number of works are devoted to the photocatalytic oxidation of various dyes [14, 15].

In the photocatalytic method of water purification, titanium dioxide is used in most cases. Titanium dioxide TiO$_2$ is one of the most common photocatalysts due to its stability, relatively high activity, and environmental safety [16, 17]. This compound occurs in three phases: anatase (tetragonal), rutile (tetragonal), and brookite (orthorhombic). The anatase phase is considered to be the most photocatalytically active than the rutile phase due to the higher (by 0.1 eV) position of the Fermi level, due to which the electrons have a higher reduction potential [18]. On the other hand, rutile has a smaller band gap (3.0 eV) compared to anatase (3.2 eV) [19], which contributes to the absorption of light with a longer wavelength [20]. Previously, in our works, a strong influence of the phase composition of titanium dioxide on its photocatalytic activity was shown [21, 22]. An affordable way to modify titanium dioxide is high-energy ball milling. During high-energy milling,

various processes can occur, including the formation of structural defects, phase transformations, morphology changes, and particle fragmentation [23].

In this work, photocatalysts based on titanium dioxide with improved physicochemical properties were synthesized by a simple and cost-effective method of high-energy milling of commercially available anatase. These samples were successfully tested in the photocatalytic oxidation of methylene blue dye under the action of UV irradiation. The influence of milling parameters on the photocatalytic and adsorption properties of the samples was revealed.

2. Experimental

2.1. Photocatalyst synthesis

Anatase titanium dioxide (Sigma Aldrich, composition: anatase – 98 wt.% rutile – 2 wt.%, 99.8% purity) was used as the initial powders (A0 sample). To modify the initial titanium dioxide powders, high-energy ball milling was used in Retsch PM 200 planetary ball mill. The high-strength ceramics, namely zirconium dioxide ZrO_2 stabilized with yttrium oxide Y_2O_3 was chosen as the material for the milling bowls and balls to minimize sample contamination during milling. The optimal mass ratio of milling balls and powders, namely 10:1, was chosen to effectively obtain the smallest nanoparticle size. Isopropyl alcohol was used as the milling liquid. To prevent the formation of rutile during milling, a special mode was chosen in this experiment: rotation speed of support disks 500 rpm at milling duration of 4 and 8 h with direction reversal every 10 minutes and a pause of 15 minutes. The obtained samples of anatase after mechanical activation for different milling times are designated A4 and A8, respectively.

2.2. Photocatalyst characterization

X-ray phase analysis of the initial and milled powders was performed in $CuK_{\alpha1,2}$ radiation using XRD-7000 (Shimadzu, Japan) autodiffractometer in the Bragg–Brentano geometry in the step-by-step scanning mode with $\Delta(2\theta) = 0.02°$ in the angle range 2θ from 10 to 120° with high statistics. The "Powder Standards Database – ICDD, USA, Release 2016" was used to identify the phases. Phase analysis was carried out using the Powder Cell 2.4 program. The dimensional and deformation contributions to the reflection broadening were determined by the Williamson–Hall method.

The specific surface area of all samples was measured using a Nova 1200e analyzer (Quantachrome Instruments, USA) implementing the Brunauer–Emmett–Teller (BET) method with preliminary degassing at 150 °C for 60 min.

Optical properties were studied by using FS-5 spectrofluorometer (Edinburgh Instruments) equipped by arc Xe-lamp (450 W), photomultiplier and integrating sphere. Spectroscopic measurements were done in the range of 250 – 850 nm at ambient temperature. Optical polytetrafluoroethylene was used as a white standard for diffuse reflectance. Processing of experimental spectra was performed using the Kubelka–Munch function.

X-ray photoelectron spectroscopy (XPS) was used to study the chemical composition of the surface of the photocatalysts with the use of photoelectron spectrometer SPECS Surface Nano Analysis GmbH (Berlin, Germany) using non-monochromatized AlK_α radiation ($hv = 1486.61$ eV). Data processing was carried out using the CasaXPS software package. Transmission electron microscopy (TEM) was used to study the structure and microstructure of the catalysts using a ThemisZ electron microscope (Thermo Fisher Scientific, Waltham, MO, USA).

The structure and microstructure of the samples were studied by high-resolution transmission electron microscopy (HRTEM) on a ThemisZ dual-corrector transmission electron microscope (Thermo Fisher Scientific, USA). Images were recorded using a Ceta 16 CCD array (Thermo Fisher Scientific, USA). The instrument is equipped with a SuperX (Thermo Fisher Scientific, USA) energy-dispersive characteristic X-ray spectrometer (EDX) with a semiconductor Si detector with an energy resolution of 128 eV.

2.3. Photocatalytic experiments

The photocatalytic reactor and emission spectra of the light source are shown in Fig. 1.

An aqueous solution of methylene blue with a concentration of $2 \cdot 10^{-4}$ M for carrying out photocatalytic oxidation was diluted 10 times and adjusted to pH = 7 with a NaOH solution with a concentration of 0.01 M. The pH of the stock solution was measured with an Ohaus Starter ST3100 pH meter. A suspension consisting of an aqueous solution of methylene blue with a volume of 100 ml and a photocatalyst with a mass of 50 mg was placed in a photocatalytic reactor and processed in an ultrasonic bath "Sapphire" UZV-1.3/2. Next, the reactor was removed for 60 minutes in a dark place for efficient adsorption of methylene blue on the catalyst. After adsorption, the photocatalytic reactor was illuminated by a LED with a wavelength of 365 nm (2 mW cm^{-2}) for 3 hours. Samples of methylene blue with a volume of 3 ml were taken before and after adsorption, as well as every hour during illumination. To obtain a pure solution without catalyst impurities, the samples were filtered using hydrophobic membrane filters. Samples were analyzed by UV-Vis spectroscopy on Shimadzu UV-2501 PC spectrophotometer.
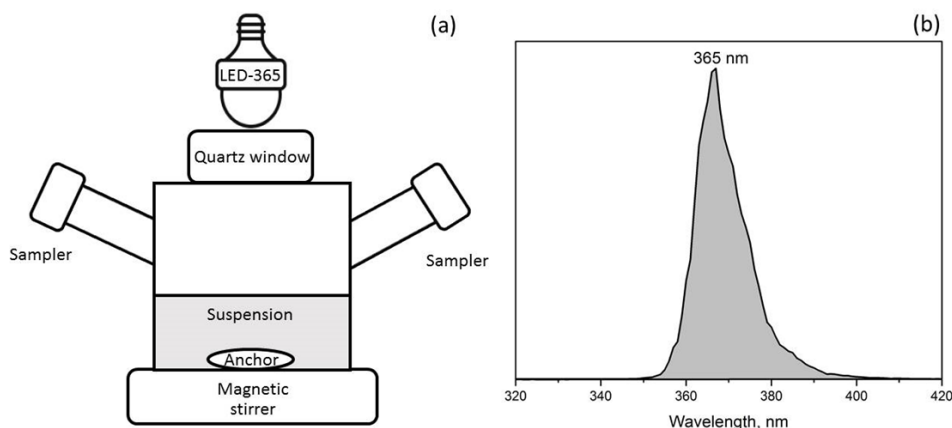
FIG. 1. Photocatalytic reactor (a), emission spectra of the light source (b)

3. Results and discussion

3.1. Characterization of photocatalyst samples

A sample of commercial anatase before milling and photocatalysts synthesized by ball milling the original TiO_2 were examined by XRD (Fig. 2a). The phase composition and textural properties of photocatalysts are presented in Table 1.
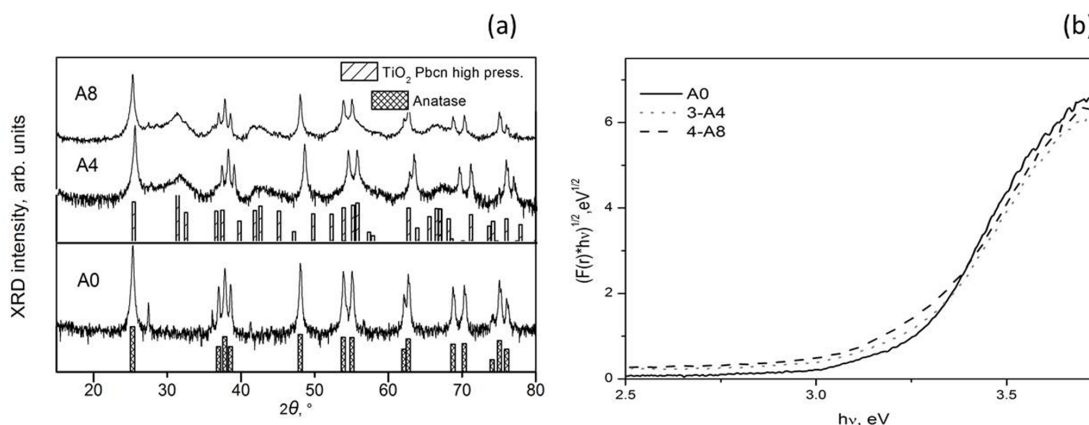

FIG. 2. XRD (a), diffuse reflectance spectra in Tauc's plot (b) of the samples

The original sample A0 is a standard anatase (I41/amd) with rutile impurities. Analysis by XRD shows that the ball milling of anatase proceeds with the formation of several modifications of TiO_2. After 4 hours of anatase milling, in addition to the standard anatase phase (I41/amd), the formation of a high-pressure phase (Pbcn) – 27 wt.%, anatase monoclinic phase (C2/m) – 3 wt.% and a standard rutile phase (P42/ mnm) – 1 wt.% were observed. Milling up to 8 hours leads to an increase in the content of the high-pressure phase up to 24 wt. %, a decrease in the average particle size and an increase in the specific surface area from 8 to 31 m^2/g.

To analyze the optical properties of the samples, diffuse reflectance spectra of photocatalysts were obtained. The band gap of the studied catalysts was determined using the Kubelka–Munk function, the calculation was performed for an indirect ($n = 2$) allowed transition (Fig. 2b). An analysis of the dependences showed that anatase milling does not lead to significant changes in the band gap of the catalysts; band gap energy is about 3.2 eV, which is typical for the anatase modification of titanium dioxide [24].

The surface properties of photocatalysts A0, A4, and A8 were studied by XPS. The relative concentrations (atomic ratios) of the elements in the surface layer of the samples, as well as the values of the Ti2p, O1s, and C1s binding energies, determined on the basis of XPS data, are presented in Table 2.

The Ti2p spectra of the studied samples are shown in Fig. 3a. As is known, the 2p level of titanium is split into two sublevels $Ti2p_{3/2}$ and $Ti2p_{1/2}$ due to the spin-orbit interaction; the spin-orbit splitting is 5.66 eV. The $Ti2p_{3/2}$ peak has a symmetrical shape, and the $Ti2p_{3/2}$ binding energy is 459.0 eV, which corresponds to Ti in the Ti^{4+} state in the TiO_2 structure. In the literature, $Ti2p_{3/2}$ binding energies are given for TiO_2 in the range of 458.7 – 459.2 eV, while for Ti in the Ti^{3+} state, in the range of 456.2 – 457.4 eV [25–29]. Also, in the Ti2p spectra of titanium of all samples, except for A0,

TABLE 1. Phase composition and textural, adsorption, and photocatalytic characteristics of the tested catalysts

Sample	Phase composition		wt. %	CSR, nm	S_{BET}, m²/g	E_g, eV	$(C_0 - C)/C_0$, % after adsorption	$(C_0 - C)/C_0$, % after photocatalysis
A0	Anatase	*I*41/*amd*	98	100	8	3.22	32	89
	Rutile	*P*42/*mnm*	2	>100				
A4	Anatase	*I*41/*amd*	69	81	16	3.22	79	87
	Anatase	*Pbcn*	27	—				
	Anatase	*C*2/*m*	3	—				
	Rutile	*P*42/*mnm*	1	53				
A8	Anatase	*I*41/*amd*	72	80	31	3.21	58	84
	Anatase	*Pbcn*	24	8				
	Anatase	*C*2/*m*	2	—				
	Rutile	*P*42/*mnm*	2	—				
Evonik P25	Anatase	*I*41/*amd*	85	19	55	3.14	9	96
	Rutile	*P*42/*mnm*	15	30				

TABLE 2. Relative atomic concentrations of elements[1] in the surface layer of the studied samples, as well as the Ti2p, O1s, and C1s binding energies (eV)

No.	Sample	[Ti³⁺]	[O_x]	[C]	[O]	Binding energy, eV		
						Ti³⁺ Ti$2p_{3/2}$	O*1s*	C*1s*
1	A0	0.01	2.56	2.38	3.25	—	530.3	285.3
2	A4	0.08	2.55	4.81	3.35	457.8	530.3	285.2
3	A8	0.11	2.47	6.18	3.56	457.8	530.3	285.2

[1]All correlations are normalized to [Ti]

a low-intensity doublet is observed in the region of lower binding energies (the binding energy of Ti2p$_{3/2}$ is 457.8 eV), which, according to the literature data, can be attributed to Ti in the Ti³⁺ state.

The O1s spectra are shown in Fig. 3b. The spectra are described by several peaks corresponding to oxygen in different environments, so the O1s peak in the region of 530.3 eV undoubtedly refers to oxygen in the TiO₂ structure [25–29]. The peak in the O1s spectra in the region of 531.9 eV for samples of series A refers to the surface OH-, sulfate/sulfite, and phosphate groups; the peak in the region and 533.6 eV refers to adsorbed water.

In order to show the transformation of the properties of the samples during milling, HRTEM images of all photocatalysts were obtained.

According to the HRTEM data, sample A0 consists of rounded particles with sizes on the order of 100 nm. On the surface of the particles, lamellar particles with sizes of 5 – 10 nm, also related to TiO₂, are observed. The analysis of interplanar distances showed the presence of the anatase phase and did not reveal defects or impurities in the composition of rounded particles, however, it should be noted that an amorphous layer is observed on the surface, this type can be attributed to contamination with carbonaceous deposits (Fig. 4a–b). HRTEM images of sample A4 are shown in Fig. 4c–d. In this sample, a large number of TiO₂ particles with sizes of about 10 nm appear on the surface of large agglomerates, while some of the fine particles also form agglomerates with sizes of about 100 nm. The study of interplanar distances showed that the nanoparticles of the main phase can be attributed to the anatase modification, and the precipitated phase to the rutile modification. This is displayed in the figures as distances of 3.3 Å for rutile and 3.5 Å for anatase. According to HRTEM data (Fig. 5), in sample A8, the content of the rutile phase increases, some of these particles agglomerate with the formation of lamellar disordered defective particles with a microdomain structure. An analysis of the interplanar
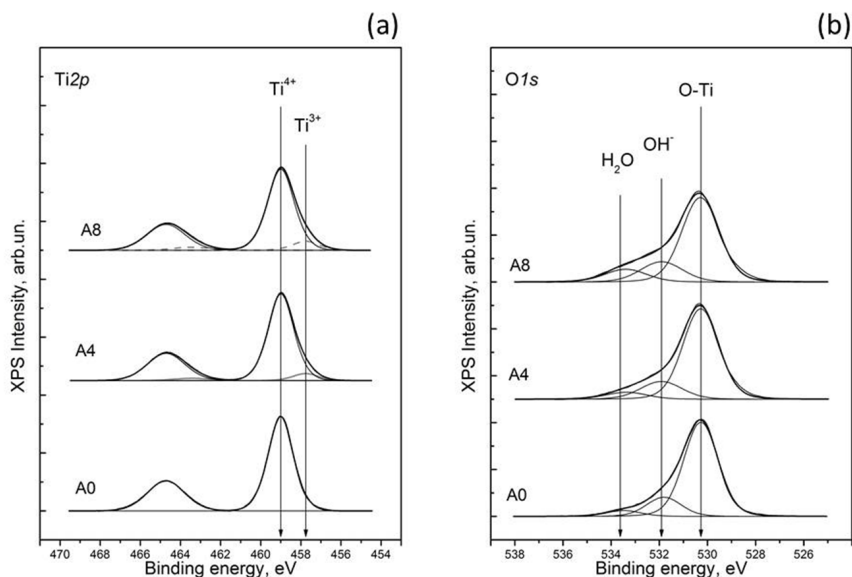
FIG. 3. XPS Ti2p (a), O1s (b) spectra of the samples

distances did not reveal the formation of new phases. Elemental mapping also shows that the sample is composed of titanium dioxide.

In general, according to the characterization by a complex of physicochemical methods of samples A0, A4, A8, the following conclusion can be made that the milling of commercial anatase leads to phase transformations and the formation of several phases of titanium dioxide, namely the high-pressure phase, the monoclinic phase of anatase and rutile, in addition there is a change in the crystalline size and the value of the specific surface area from 8 to 31 m^2/g. It has been established that defects are introduced into the system during grinding, which is confirmed by XPS and HRTEM data. It is believed that this defective structure improves the adsorption and catalytic properties of materials.

3.2. Photocatalytic activity

The activity of all the studied samples was investigated in the photocatalytic oxidation of the methylene blue dye under the action of UV radiation with a wavelength of 365 nm. Optical densities of the dye solutions before and after irradiation at a wavelength of 666 nm were used to calculate the decoloration degree of the dye. For comparison, photocatalytic oxidation was carried out using the most commonly used commercial photocatalyst TiO_2 Degussa P25 (anatase/rutile).
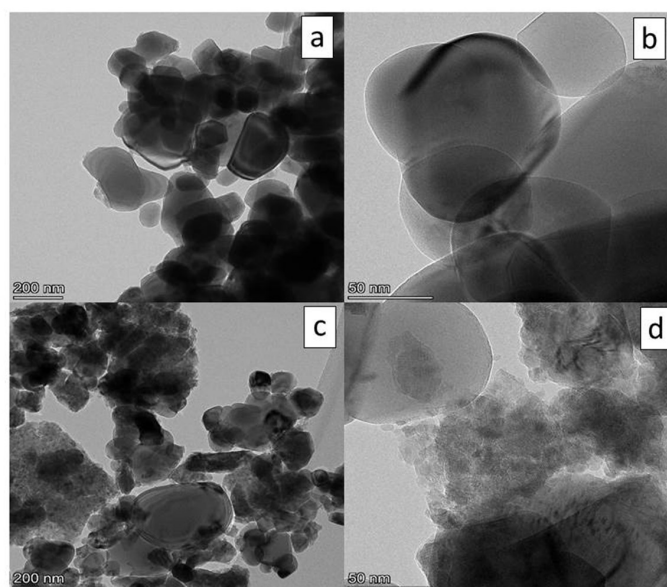

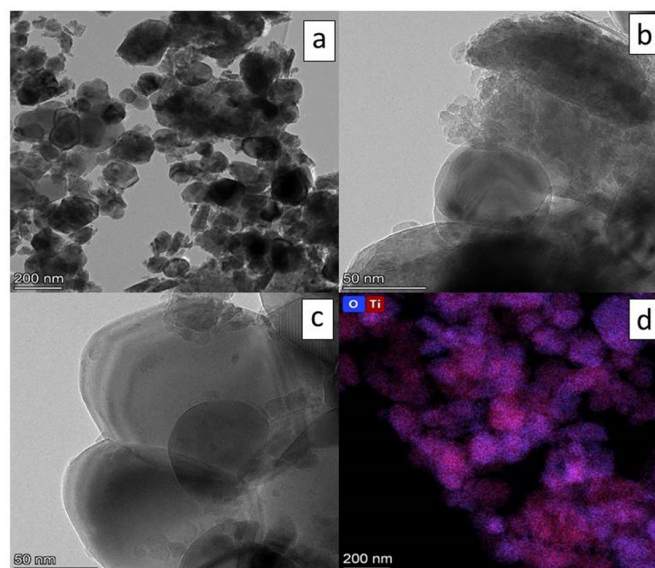FIG. 4. HRTEM images of sample A0 (a–b top) and A4 (c–d bottom)

FIG. 5. HRTEM images (a–c) and EDX mapping (d) of sample A8

Substrate adsorption and photocatalytic oxidation data are presented in Table 1; kinetic dependences of photocatalytic oxidation are presented in Fig. 6.

It can be seen that in the blank experiment without a photocatalyst, no degradation of the dye under the action of UV-irradiation is observed. At the same time, with all samples of titanium dioxide, including Degussa P25, almost complete degradation of the MB dye occurred in an hour of irradiation. A significant difference is the much stronger adsorption occurring both in the presence of sample A0, and especially in the presence of samples A4 and A8. Thus, almost 80 % of the dye was degraded during an hour of dark adsorption on sample A4. It is worth paying attention to the UV-vis spectra of the reaction suspension obtained during experiments with the A8 photocatalyst. It can be seen that after the stage of dark adsorption and at the first stages of oxidation, adsorption in the 400 – 600 nm region increases, which can be explained by the rapid formation of intermediate oxidation products. According to the literature, high performance liquid chromatography revealed the formation of some dyes of the thiazine series, such as azures and thionine, during irradiation of methylene blue solutions in the presence of modified titania [30, 31].

It can be concluded that the milling of anatase A0 significantly increases its adsorption properties, which, of course, is associated with an increase in the specific surface area of the samples and a decrease in the size of titanium dioxide crystallites. In addition, the defectiveness of the synthesized samples is also a beneficial for its adsorption and photocatalytic properties. It should be noted that from a practical point of view, fast adsorption with further oxidation of the pollutant, as occurs in the case of samples A4 and A8, is more advantageous than slow adsorption with further faster photocatalytic oxidation, as in the case of commercial Degussa P25, because the main task is to quickly neutralize the release of harmful substances.

4. Conclusions

In conclusion, in this work, a new method for the formation of active photocatalysts based on high-energy ball milling of commercial anatase was proposed. It has been shown that milling leads to a complication of the phase composition of anatase with the formation of new high-pressure phases; the dispersion of particles and the specific surface of the material increase, and defects also appear. It was shown that the materials synthesized in this work have unique properties and phase composition. The samples obtained by grinding showed high activity in the photocatalytic oxidation of the dye, methylene blue, under the UV irradiation. The adsorption properties of the obtained materials significantly exceed those of the commercial TiO_2 Degussa P25, which leads to good prospects for the use of these materials for environmentally friendly water purification from pollution of various classes.

References

[1] Reddy N.R., Reddy P.M., Jyothi N., Kumar A.S., Jung J.H., Joo S.W. Versatile TiO_2 bandgap modification with metal, non-metal, noble metal, carbon material, and semiconductor for the photoelectrochemical water splitting and photocatalytic dye degradation performance. *J. of Alloys and Compounds*, 2023, **935**, 167713.

[2] Jo W.K., Tayade R.J. Recent developments in photocatalytic dye degradation upon irradiation with energy-efficient light emitting diodes. *Chinese J. of Catalysis*, 2014, **35** (11), P. 1781–1792.

[3] Ajmal A., Majeed I., Malik R.N., Idriss H., Nadeem M.A. Principles and mechanisms of photocatalytic dye degradation on TiO_2 based photocatalysts: A comparative overview. *RSC Advances*, 2014, **4** (70), P. 37003–37026.
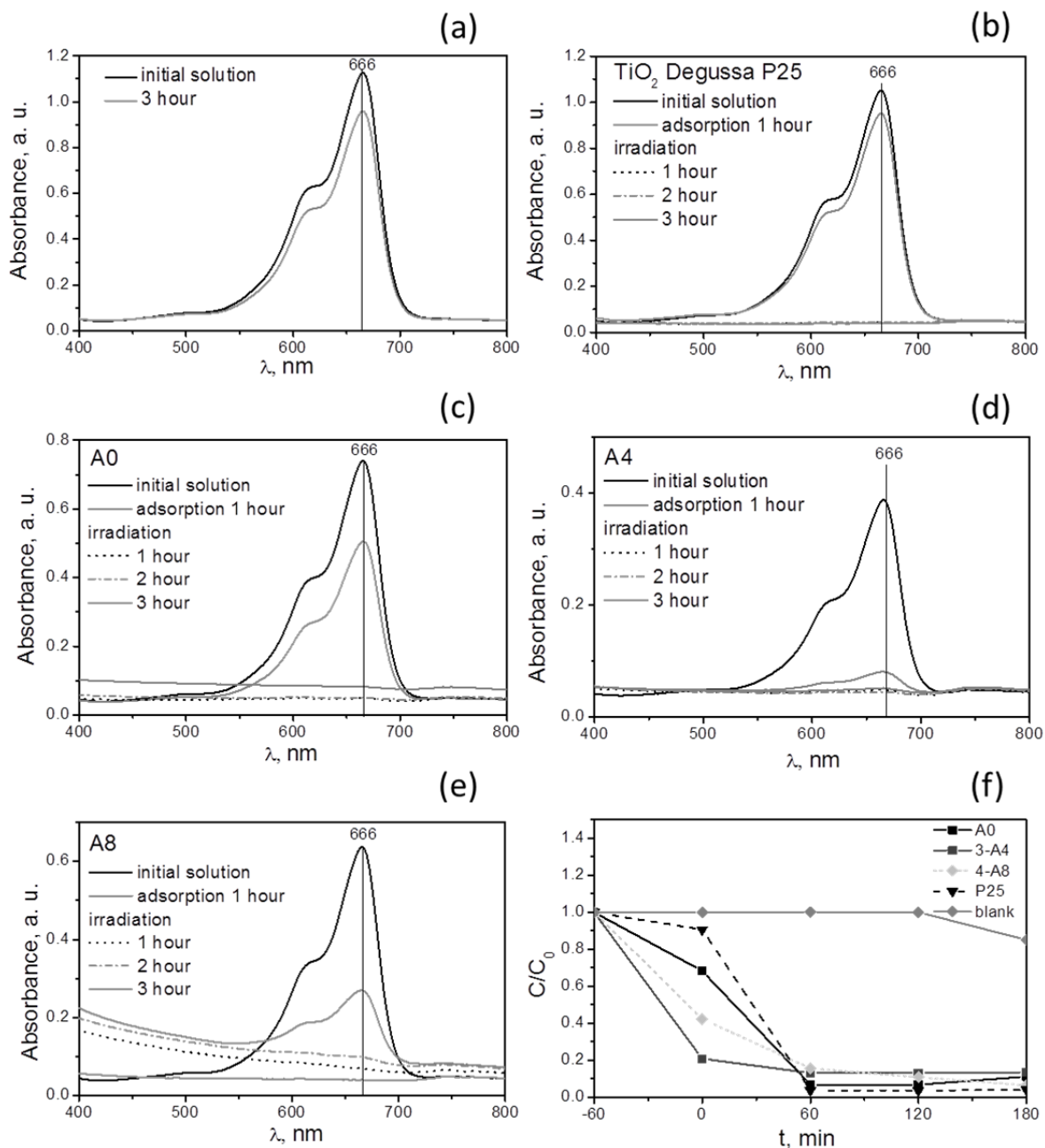
FIG. 6. Absorption spectra of methylene blue before and after the photocatalytic reaction without photocatalyst (a), with photocatalyst: P25 (b), A0 (c), A4 (d), A8 (e), kinetic dependences of photocatalytic oxidation of the samples (f)

[4] Bensalah N., Alfaro M.A.Q., Martínez-Huitle C.A. Electrochemical treatment of synthetic wastewaters containing Alphazurine A dye. *Chemical Engineering J.*, 2009, **149** (1–3), P. 348–352.

[5] Turhan K., Turgut Z. Decolorization of direct dye in textile wastewater by ozonization in a semi-batch bubble column reactor. *Desalination*, 2009, **242** (1–3), P. 256–263.

[6] Gosetti F., Gianotti V., Angioi S., Polati S., Marengo E., Gennaro M.C. Oxidative degradation of food dye E133 Brilliant Blue FCF: Liquid chromatography-electrospray mass spectrometry identification of the degradation pathway. *J. of Chromatogr. A*, 2004, **1054** (1–2), P. 379–387.

[7] Rauf M.A., Ashraf S.S. Fundamental principles and application of heterogeneous photocatalytic degradation of dyes in solution. *Chemical Engineering J.*, 2009, **151** (1–3), P. 10–18.

[8] Adhikari S., Sarkar D. Metal oxide semiconductors for dye degradation. *Materials Research Bulletin*, 2015, **72**, P. 220–228.

[9] Mohibbul M., Bahnemann D., Muneer M. Photocatalytic Degradation of Organic Pollutants: Mechanisms and Kinetics. In: *Organic Pollutants Ten Years After the Stockholm Convention – Environmental and Analytical Update*, Ed. T. Puzyn, A. Mostrag-Szlichtyng, 2012.

[10] Malato S., Blanco J., Fernández-Alba A.R., Agüera A. Solar photocatalytic mineralization of commercial pesticides: Acrinathrin. *Chemosphere*, 2000, **40** (4), P. 403–409.

[11] Percherancier J.P., Chapelon R., Pouyet B. Semiconductor-sensitized photodegradation of pesticides in water: the case of carbetamide. *J. of Photochemistry and Photobiology, A: Chemistry*, 1995, **87** (3), P. 261–266.

[12] Doong R.A., Chang W.H. Photoassisted titanium dioxide mediated degradation of organophosphorus pesticides by hydrogen peroxide. *J. of Photochemistry and Photobiology A: Chemistry*, 1997, **107** (1–3), P. 239–244.

[13] Kerzhentsev M., Guillard C., Herrmann J.M., Pichat P. Photocatalytic pollutant removal in water at room temperature: Case study of the total degradation of the insecticide fenitrothion (phosphorothioic acid O,O-dimethyl-O-(3-methyl-4-nitro-phenyl) ester). *Catalysis Today*, 1996, **27** (1–2), P. 215–220.

[14] Akpan U.G., Hameed B.H. Parameters affecting the photocatalytic degradation of dyes using TiO_2-based photocatalysts: A review. *J. of Hazardous Materials*, 2009, **170** (2–3), P. 520–529.

[15] Bachina A.K., Popkov V.I., Seroglazova A.S., Enikeeva M.O., Kurenkova A.Yu., Kozlova E.A., Gerasimov E.Yu., Valeeva A.A., Rempel A.A. Synthesis, Characterization and Photocatalytic Activity of Spherulite-like r-TiO_2 in Hydrogen Evolution Reaction and Methyl Violet Photodegradation. *Catalysts*, 2022, **12** (12), 1546.

[16] Rempel A.A., Valeeva A.A. Nanostructural titanium dioxide for medical chemistry. *Russ. Chem. Bull.*, 2019, **68**, P. 2163–2171.

[17] Postnova I., Kozlova E., Cherepanova S., Tsybulya S., Rempel A., Shchipunov Y. Titania synthesized through regulated mineralization of cellulose and its photocatalytic activity. *RSC Advances*, 2015, **5** (12), P. 8544–8551.

[18] Bickley R.I., Gonzalez-Carreno T., Lees J.S., Palmisano L., Tilley R.J.D. A structural investigation of titanium dioxide photocatalysts. *J. of Solid State Chemistry*, 1991, **92** (1), P. 178–190.

[19] Rempel A.A., Valeeva A.A., Vokhmintsev A.S., Weinstein I.A. Titanium dioxide nanotubes: synthesis, structure, properties and applications. *Russ. Chem. Rev.*, 2021, **90** (11), P. 1397–1414.

[20] Hurum D.C., Agrios A.G., Gray K.A., Rajh T., Thurnauer M.C. Explaining the enhanced photocatalytic activity of Degussa P25 mixed-phase TiO_2 using EPR. *J. of Physical Chemistry B*, 2003, **107** (19), P. 4545–4549.

[21] Saraev A.A., Kurenkova A.Y., Gerasimov E.Y., Kozlova E.A. Broadening the Action Spectrum of TiO_2-Based Photocatalysts to Visible Region by Substituting Platinum with Copper. *Nanomaterials*, 2022, **12** (9), 1584.

[22] Kurenkova A.Y., Kremneva A.M., Saraev A.A., Murzin V., Kozlova E.A., Kaichev V.V. Influence of Thermal Activation of Titania on Photoreactivity of Pt/TiO_2 in Hydrogen Production. *Catalysis Letters*, 2021, **151** (3), P. 748–754.

[23] Ordinartsev D.P., Pechishcheva N.V., Valeeva A.A., Zaitseva P.V., Korobitsyna A.D., Belozerova A.A., Sushnikova A.A., Petrova S.A., Shunyaev K.Yu., Rempel' A.A. Nanosized Titania for Removing Cr(VI) and As(III) from Aqueous Solutions. *Russian J. of Physical Chemistry A*, 2022, **96** (11), P. 2408–2416.

[24] Reddy K.M., Manorama S.V., Reddy A.R. Bandgap studies on anatase titanium dioxide nanoparticles. *Materials Chemistry and Physics*, 2003, **78** (1), P. 239–245.

[25] Luan Z., Maes E.M., Van Der Heide P.A.W., Zhao D., Czernuszewicz R.S., Kevan L. Incorporation of titanium, into mesoporous silica molecular sieve SBA-15. *Chemistry of Materials*, 1999, **11** (12), P. 3680–3686.

[26] Hasegawa Y., Ayame A. Investigation of oxidation states of titanium in titanium silicalite-1 by X-ray photoelectron spectroscopy. *Catalysis Today*, 2001, **71** (1–2), P. 177–187.

[27] Agnoli S., Barolo A., Finetti P., Sedona F., Sambi M., Granozzi G. Core and valence band photoemission study of highly strained ultrathin NiO films on Pd(100). *J. of Physical Chemistry C*, 2007, **111** (9), P. 3736–3743.

[28] Kaichev V.V., Popova G.Ya., Chesalov Yu.A., Saraev A.A., Zemlyanov D.Y., Beloshapkin S.A., Knop-Gericke A., Schlögl R., Andrushkevich T.V., Bukhtiyarov V.I. Selective oxidation of methanol to form dimethoxymethane and methyl formate over a monolayer V_2O_5/TiO_2 catalyst. *J. of Catalysis*, 2014, **311**, P. 59–70.

[29] Kaichev V.V., Chesalov Yu.A., Saraev A.A., Klyushin A.Yu., Knop-Gericke A., Andrushkevich T.V., Bukhtiyarov V.I. Redox mechanism for selective oxidation of ethanol over monolayer V_2O_5/TiO_2 catalysts. *J. of Catalysis*, 2016, **338**, P. 82–93.

[30] Rauf, M.A., Meetani, M.A., Khaleel A., Ahmed, A. Photocatalytic degradation of methylene blue using a mixed catalyst and product analysis by LC/MS. *Chemical Engineering J.*, 2010, **157**, P. 373–378.

[31] Markovskaya, D.V., Zhurenok, A.V., Kurenkova, A.Y., Kremneva, A.M., Saraev, A.A., Zharkov, S.M., Kozlova, E.A., Kaichev, V.V. New Titania-Based Photocatalysts for Hydrogen Production from Aqueous-Alcoholic Solutions of Methylene Blue. *RSC Advances*, 2020, **10**, P. 34137–34148.

Information about the authors:

Ekaterina A. Kozlova – Institute of Metallurgy, Ural Branch of the Russian Academy of Sciences, 620016 Amundsena St., 101, Ekaterinburg, Russia; Boreskov Institute of Catalysis, Siberian Branch of the Russian Academy of Sciences, 630090, pr. Ak. Lavrentieva, 5, Novosibirs, Russia; ORCID 0000-0001-8944-7666; kozlova@catalysis.ru

Albina A. Valeeva – Institute of Solid State Chemistry, Ural Branch of the Russian Academy of Sciences, 620108, Pervomayskaya 91, Ekaterinburg, Russia; ORCID 0000-0003-1656-732X; anibla_v@mail.ru

Anna A. Sushnikova – Institute of Metallurgy, Ural Branch of the Russian Academy of Sciences, 620016 Amundsena St., 101, Ekaterinburg, Russia; ORCID 0000-0002-7604-5673; sushnikova.ann@gmail.com

Angelina V. Zhurenok – Boreskov Institute of Catalysis, Siberian Branch of the Russian Academy of Sciences, 630090, pr. Ak. Lavrentieva, 5, Novosibirs, Russia; ORCID 0000-0003-3908-1963; angelinazhurenok@gmail.com

Andrey A. Rempel – Institute of Metallurgy, Ural Branch of the Russian Academy of Sciences, 620016 Amundsena St., 101, Ekaterinburg, Russia; ORCID 0000-0002-0543-9982; rempel.imet@mail.ru

Conflict of interest: the authors declare no conflict of interest.